

QUANTITATIVE LITHOLOGY: AN APPLICATION FOR OPEN AND CASED HOLE SPECTROSCOPY

Susan L. Herron and Michael M. Herron
Schlumberger-Doll Research
Old Quarry Road
Ridgefield, CT 06877-4108

ABSTRACT

A new quantitative lithology interpretation is based on elemental concentrations available from logs. The concentration logs are obtained from single, induced-neutron gamma ray spectrometers, thus differentiating this work from earlier geochemical interpretations which required additional sondes for the measurement of aluminum and potassium. The new interpretation offers considerable advantages over conventional logs.

This new interpretation is based on a recently acquired data base. Fourier transform infrared mineralogy and chemical compositions were measured on over 400 samples to examine the relationships between lithology and a number of geochemical signatures, including gamma ray, the gamma ray components Th, U, and K and other loggable elements. The results show that in individual wells, gamma ray correlates roughly with total clay content, but a closer analysis exposes the inherent weaknesses in clay estimation. Breaking gamma ray down into its individual components brings little improvement to the clay estimation compared to that possible from a different suite of geochemical logs.

The study reveals a strong linear relationship between aluminum and total clay concentrations. It is characterized by a near-zero intercept and a common slope. Unfortunately, the measurement of aluminum by logging devices has proven to be difficult and expensive. This study introduces a technique whereby the elements silicon, calcium and iron can be used to produce as accurate an estimation of clay as from aluminum. A general algorithm for predicting clay from these three elements is presented. An example of how the algorithm can be optimized is also provided.

Carbonate concentrations are determined from the calcium concentration log with an accuracy that is not available from any other logging devices. Finally, the remainder of the formation is composed of quartz, feldspar, and mica minerals. Examples of the new lithology interpretation are provided for both open and cased hole environments.

INTRODUCTION

The accurate determination of formation lithology from common geophysical logs is hindered by a lack of sensitivity coupled with nonunique responses to the minerals that reside in sedimentary rocks. The interpretation of lithology primarily consists of estimating fractions of shale, sand and carbonate. Shale is a kind of sedimentary rock which contains a significant amount of clay minerals, but there are many types of clay minerals with widely differing compositions and log responses, so estimations of clay, or volume of shale, often carry large uncertainties. Carbonates generate nuclear and sonic log responses that are different, but not necessarily unique, from noncarbonate minerals. A small amount of calcite cement in a sandstone is virtually impossible to reliably estimate from conventional log data.

Nuclear logs, either gamma ray, P_c , and/or a combination of neutron and density are the most commonly used logs for lithology interpretation. A desire for improved accuracy in lithological description led to the introduction of several generations of nuclear spectroscopy logs. In the openhole environment, natural gamma ray spectroscopy logs brought limited improvement to clay quantification in sandstones and carbonates and also enabled identification of marine source rocks. For the cased hole environment, induced gamma ray spectroscopy logs introduced relative elemental yields that can be used for qualitative lithological description. In an attempt to attain accurate, quantitative characterization of formation mineralogy, natural and induced spectroscopy logs were combined with an aluminum activation measurement in a single openhole tool string (Hertzog et al., 1987). These measurements were further enhanced by the geochemical oxides closure processing technique which produced quantitative concentration logs for ten elements (Hertzog et al., 1987; Schweitzer et al., 1988; Grau and Schweitzer, 1989; Grau et al., 1989). Unfortunately, the combination of three spectrometers on a single tool string is logistically difficult and costly, and the interpretation is sometimes complex.

Recent developments in research and engineering capture the essence of geochemical log data using single, induced-neutron gamma ray spectrometers. Eliminating the need for aluminum and potassium in both the derivation of elemental concentrations and in the interpretation of quantitative lithology greatly simplifies data acquisition and interpretation. The new lithological interpretations are founded on an extensive core data base. This paper provides a brief introduction to the new geochemical logging capabilities in both open and cased holes and a detailed examination of the new core-based interpretation.

ELEMENTAL CONCENTRATION LOGS

The new technique to estimate elemental concentrations from an induced-neutron gamma ray spectrometer (Herron, 1995) is an adaptation of the geochemical oxides closure model currently employed in the computation of elemental concentrations (Hertzog et al., 1987; Schweitzer et al., 1988; Grau and Schweitzer, 1989; Grau et al., 1989). The only significant modification is a change in the iron association factor to compensate for the lack of aluminum and potassium measurements. The processing has been tested on core data as well as open and cased hole spectroscopy data with promising results.

Figure 1 presents examples of elemental concentration logs from the new processing using data from an openhole Elemental Capture Spectroscopy (ECS*) sonde. This is a new spectroscopy device which uses a standard AmBe source and a BGO detector. It is combinable and can log at up to 1800 ft/hr (540 m/hr). Chemical concentrations measured on core samples are shown for comparison. Two points should be made when examining the data. The first is that since the uncorrected prompt capture yield for iron contains gamma rays from both Fe and Al, the log Fe should be approximately equal to Fe + 0.14 Al. Accordingly, the core points plotted for comparison are Fe + 0.14 Al. The second point is that the log concentrations agree well with core data.

A second example is provided from a cased hole Reservoir Saturation Tool (RST*) log acquired from a well in Venezuela (Figure 2). This example is processed using new elemental standards to derive the far detector capture yields (Roscoe et al., 1995), and corrections are made for casing and a 1.5-in. cement annulus. The results show good agreement between log concentrations and the sparse core data.

* Mark of Schlumberger

CORE DATA BASE

The development of the new quantitative lithology interpretation begins with a core data base that contains chemistry and mineralogy measurements on over 400 core plug samples from numerous wells on four continents. The wells are diverse in age and geographic location, but all are predominantly sands and shaly sands.

To analyze the samples, rocks were crushed and split with a microsplitter into chemistry and mineralogy fractions. The chemistry fraction was analyzed at X-Ray Assay Laboratories for whole rock elemental concentrations of silicon (Si), aluminum (Al), iron (Fe), calcium (Ca), magnesium (Mg), sodium (Na), potassium (K), phosphorus (P), titanium (Ti), manganese (Mn) and chromium (Cr), expressed as oxides, plus Loss on Ignition (LOI) representing total volatiles, H₂O⁺, H₂O⁻, sulfur (S), organic carbon, thorium (Th), uranium (U), gadolinium (Gd) and boron (B). A synthetic core gamma ray computed from core chemistry using the gamma ray response is given by equation (1)

$$GR = 4 Th + 8 U + 16 K \quad (1)$$

where Th and U concentrations are in ppm and K concentrations are in wt% (Ellis, 1987).

The mineralogy fraction was analyzed using a new Fourier Transform Infrared (FT-IR) procedure which simultaneously analyzes the mid-IR and far-IR frequencies. The mid-IR procedure was described in Matteson and Herron (1993). Since that time the number of mineral standards has been increased to 26 with approximately the same level of accuracy (better than ± 2 wt %). The mineral standard set includes quartz, albite, anorthite, K-feldspar, muscovite, biotite, kaolinite, illite, smectite, chlorite, glauconite, calcite, dolomite, siderite, ankerite, magnesite, aragonite, gypsum, anhydrite, hematite, barite and opal. Total clay is the sum of kaolinite, illite, smectite, chlorite and glauconite. Although there are significant amounts of mica, another layered silicate, they are not included in the total clay fraction. At high clay concentrations there is sometimes crosstalk between illite and mica phases.

EXPLORING ELEMENTAL RELATIONSHIPS

Gamma Ray and Clay. With these core data, it is possible to evaluate the relationship between total clay and the computed gamma ray on a porosity-free basis, as recently advocated by Katahara (1995). The relationship for core samples from 12 data sets is presented in Figure 3. A line connecting the origin with

100% clay and 250 API is included for visual reference. As expected, gamma ray content generally increases as clay content increases. However, there are a number of characteristics in the clay-gamma ray plots that highlight the weaknesses inherent in this approach; many of these have been recently discussed by Bhuyan and Passey (1994) and Hurst and Milodowski (1994).

The first major feature is the large range of slopes in the gamma ray versus clay plots which demonstrates the necessity for local calibration. For example, in Well 1, a linear trend would predict a maximum gamma ray value of about 100 API for the pure clay end member, whereas Well 2 would predict 500 API. For Well 12, a pure clay would have a gamma ray of only about 150 API. In several wells, either the data or an extrapolation of the data to zero clay indicate a near zero minimum gamma ray, but Well 4 has a minimum gamma ray of 30 API, and in Well 12 an extrapolation points to 70 API for minimum gamma ray. The difference between evaluating these plots and using only log data is that with core calibration the amount of clay is known, and it is possible to accurately extrapolate to zero clay. With only log data, one must choose a minimum and maximum gamma ray value without knowing the correspondence to real clay concentrations, and the picture is further complicated by porosity variations. For Well 11, the minimum gamma ray value observed on the log is about the same as the 50 API minimum computed for the core data. This value would normally be assigned to zero clay instead of the actual 25 wt% clay. Clearly, such a log interpretation would severely underestimate the clay content in the well.

The second dominant feature in Figure 3 is the scatter in the data, particularly in Wells 1-10. In these wells, even if the observed correlation between gamma ray and clay were known, the scatter in the data would produce an uncertainty of as much as ± 20 wt% clay or more. For Wells 3, 5, 7 and 9, at levels of about 20% clay, observed gamma ray values span almost the full range from clean sand to shale. The relative error is particularly large in sands.

A third and less common feature is that some wells exhibit a small dynamic range in gamma ray while clay content varies considerably. This is notable in Well 12 which is a typical offshore Gulf of Mexico example. It is also true in Wells 4 and 11.

In spite of the problems outlined above, it would be possible to make good clay predictions in Wells 2, 11 and 12 if detailed and accurate core data are available. Without such a calibration, it is doubtful that the picks for GR_{max} and GR_{min} from the log data would match the core calibration parameters.

Seeking an Elemental Alternative. The goal of this study is to identify an alternative, less subjective approach to determining clay content using elemental data available from nuclear spectroscopy logging devices. Currently the technology exists to measure elemental concentrations from natural radioactivity (Th, U and K), neutron activation (Al), and capture gamma ray spectroscopy (Si, Ca, Fe, Ti, Gd and S). The ability to compute absolute concentrations from induced gamma ray spectroscopy yields (Herron, 1995) is a new development which justifies a fresh look at relationships between chemical elements and lithological fractions.

Figure 4 shows a comparison of clay with all available logging elements (except sulfur) for Well 3. The three components of natural gamma ray, Th, U and K are presented in the first row. Thorium and uranium show wide scatter and little correlation with clay. In this well, potassium shows a strong correlation with clay, but examination of data from four other wells in the field reveals that this correlation breaks down entirely in sands containing less than 25% clay.

The second row of Figure 4 begins with a comparison of clay with aluminum. In Well 3, aluminum displays a strong relationship with total clay. The remaining elements in this figure are some that can be obtained by prompt thermal neutron capture spectroscopy logging devices. The two elements remaining in the second row of the figure are titanium and gadolinium. These elements are commonly enriched in shales, but they show only a loose correlation with total clay.

The third row holds the key to a new technique for estimating clay. It begins with silicon, which is a major constituent of rock forming minerals. Although silicon is commonly associated with quartz, it is actually the second most abundant element after oxygen in both sandstones and shales. Because it is a major element, its abundance is not affected by trace minerals, and concentrations form a smooth continuum between high silicon sandstones and medium silicon shales. For reference, quartz has 46.8 wt% silicon. The next element is iron, which has numerous associations, including heavy minerals such as siderite and pyrite and the clay minerals illite, chlorite and glauconite. High concentrations of the heavy iron minerals can interrupt the smooth relationship between silicon and clay content. The final element is calcium which is mainly associated with the carbonate minerals calcite and dolomite. The low calcium concentrations indicate the absence of carbonate minerals in Well 3.

The same type of comparison between total clay and elemental concentrations is presented in Figure 5 for

Well 5. For this well, none of the individual elements (Th, U and K) contributing to natural gamma ray is any better correlated with clay than total gamma ray. In contrast, aluminum again shows a tight correlation with clay content. Silicon again shows a strong negative correlation with clay, but there are two data points which clearly deviate from the major trend. These two samples contain 13 and 38 wt% siderite (FeCO_3) as reflected by the two high iron points. As in Well 3, the near absence of calcium reflects the absence of calcite and dolomite.

A final example of the element-clay comparisons is presented in Figure 6 for Well 6. In this well, thorium and potassium exhibit positive correlations with clay, but the degree of scatter precludes the use of these elements for accurate clay prediction, especially at low clay contents. Aluminum again shows a strong positive correlation with clay. Silicon again shows a negative correlation with clay, but the impact of carbonate minerals on the silicon-clay curve is much more obvious. There are many samples with high calcium reflecting calcite concentrations that range from 0 to 85 wt%. This mineral assemblage produces a ternary composition diagram in the silicon-clay plot with the vertices representing pure carbonate, clean sand, and shale.

Summarizing the observations in Figures 4 through 6, it appears that aluminum is the best single elemental indicator of clay. Silicon shows a complementary anti-correlation to clay content, but the simple linear relationship between silicon and clay is distorted by carbonate minerals. The carbonate content is chemically represented by calcium and/or iron. These trends are typical of those observed in the other data sets.

Having observed the strong relationship between aluminum and clay, it is useful to examine the data for all 12 wells, as shown in Figure 7. In 10 of the 12 wells, the slope of the aluminum-clay plot is nearly constant. In 9 of the 12 wells, the intercept of the aluminum-clay linear relationship is essentially zero. Comparison between Figure 7 and Figure 3 shows that aluminum is a much better clay estimator than gamma ray in most wells. This is true even when a porosity-free core calibration is available for gamma ray, and it is especially true in the sands.

The improvement of aluminum over gamma ray is marginal in Well 8, but it is significant for the cleanest sands. In Wells 11 and 12, the aluminum and gamma ray are comparable clay indicators if the core calibration is known. However, a log interpreter who equates the minimum gamma ray response with zero

clay introduces a 20 to 25 wt% error in the clay estimation.

Aluminum has an even more striking relationship with the sum of clay plus mica. This is demonstrated in Figure 8. Improvements in the correlation with aluminum are most notable in Wells 7 and 8, and the effects are most obvious in the shales. The lines drawn in Figure 8 represent a slope of 6.4 and the relationship for the first 10 wells has a correlation coefficient of 0.98. It is possible that some of the differences between Figures 7 and 8 are due to analytical crosstalk between illite and mica phases in shales. The decision to include or exclude mica from the clay fraction depends on the application. Since micas do not contribute significantly to clay counter-ion conductivity, they are not generally included in saturation interpretation. On the other hand, like clays, micas can be detrimental to formation productivity.

There are several reasons why aluminum correlates strongly with total clay mineral content. Clays are aluminosilicates; aluminum is a major element in and an integral part of the chemical composition of all clays. This is very different from the case of thorium and uranium which occur at trace (ppm) levels and are not structural components of the clays. Of course, the clay-Al relationship is a simplified picture and is not expected to be perfect. Different clay minerals have different Al concentrations and there are important non-clay minerals that contain aluminum.

Relationship between Al and Si, Ca, Mg and Fe. Although aluminum is the best element for clay estimation, its measurement in a borehole is accomplished by induced neutron activation and currently requires a chemical source, two gamma ray spectrometers, and an independent measurement of formation capture cross section, making it an expensive measurement. Fortunately, an alternative exists due to the complementary relationship between aluminum and the elements silicon, calcium, magnesium and iron. This relationship will be illustrated in Figure 9, which combines elemental data from all 12 data sets into three plots. Samples containing more than 2 wt% organic carbon are excluded.

Earlier, Figures 4 to 6 showed that as clay increases, silicon decreases. Therefore, as aluminum increases, silicon decreases. In Figure 9a, silicon is converted to SiO_2 (by multiplying by 2.139) and subtracted from 100. Now, we see that as Al increases, $100-\text{SiO}_2$ also increases. In this presentation, carbonate minerals drive the data toward Al of zero and $(100-\text{SiO}_2)$ values of 100 wt%. We can use concentrations of Ca and Mg to compensate for the presence of calcite (CaCO_3) and dolomite ($\text{CaMg}(\text{CO}_3)_2$). Figure 9b shows that

concentrations of Al vary linearly when plotted against $100 - \text{SiO}_2 - \text{CaCO}_3 - \text{MgCO}_3$ concentrations and that the additional terms remove almost all of the disturbance of that major trend. The few remaining outliers are predominantly siderite or pyrite, and they can be removed as 1.99Fe where the coefficient of 1.99 is optimized on these data.

The trend in Figure 9c can be used to estimate the aluminum concentration from

$$\text{Al} = 0.34(100 - \text{SiO}_2 - \text{CaCO}_3 - \text{MgCO}_3 - 1.99\text{Fe}) \quad (2)$$

which produces estimates of Al with a correlation coefficient of 0.99 and a standard error of 0.6 wt% Al. Figure 10 presents a comparison of measured Al concentrations with those estimated from equation (2) for each of the 12 wells. Clearly, this is a robust means of estimating Al from Si, Ca, Mg and Fe.

QUANTITATIVE LITHOLOGY

Estimating Clay. The two major points from the preceding section are that Al correlates well with clay content and that aluminum concentrations can be estimated from Si, Ca, Mg and Fe. The next logical step is to estimate clay content from Si, Ca, Mg and Fe using the form of equation (2). The problem is set up to determine clay content by optimizing the slope. Samples from Wells 11 and 12 are excluded from the optimization because, as seen in Figure 7, the relationship between aluminum and clay differs significantly from the relationships observed in Wells 1 through 10. The new clay algorithm is:

$$\text{Clay} = 1.67(100 - \text{SiO}_2 - \text{CaCO}_3 - \text{MgCO}_3 - 1.99\text{Fe}) \quad (3)$$

which has a correlation coefficient of 0.94 and a standard error of 6.9 wt%. The slope of 1.67 obtained here is representative of the combined data sets. Slopes optimized on individual data sets range from a maximum of 2.0 for Well 1 to a minimum of 1.3 for Well 10.

If we solve for clay plus mica (Figure 8) instead of clay, we obtain the following equation:

$$\text{Clay} + \text{Mica} = 2.20(100 - \text{SiO}_2 - \text{CaCO}_3 - \text{MgCO}_3 - 1.99\text{Fe}) \quad (4)$$

with a correlation coefficient of 0.97 and a standard error of 6.5 wt%.

Figure 11 presents measured clay content and estimates from equation (3) for all 12 wells. The estimated clay concentrations are in good agreement with the measured values for Wells 1-7, 9 and 10. They are

almost the same as the estimates from aluminum shown in Figure 7.

For most of the first ten wells, the clay estimates portrayed in Figure 11 constitute an improvement over those attainable from gamma ray. The scatter in the estimate is drastically reduced, particularly at the low clay concentrations where clay estimation is most critical. This is especially clear in Wells 1-7 and 9 and 10. In Well 8, the estimate of clay shows a less spectacular effect relative to gamma ray, but it does offer slight improvement in the clean sands. In this well, an estimate of clay plus mica would clearly be superior to gamma ray estimates.

Equation (3) is a general algorithm for estimating clay from elemental data. It has broad applicability and does not require picks of minimum and maximum values. Unlike neutron-density separation, equation 3 is not affected by the presence of light hydrocarbons or gas. Although the slope would vary if optimized on individual data sets, the overall slope of 1.67 in equation (3) produces a good clay estimate.

For Wells 11 and 12 the clay estimated from equation 3 agrees with the measured clay in the cleanest samples but underestimates the clay content of the shales. The cleanest samples in these two wells have 20 and 28 wt% clay, and it is not obvious which way the data would trend in cleaner rocks. This is the same trend observed for these two wells in the comparison of aluminum versus clay.

The problem with the interpretation of clay from Al or from Si, Ca and Fe in Wells 11 and 12 is basically the same as the problem with interpreting gamma ray. Inherent in both interpretation schemes is the presumption that non-clay minerals do not interfere. For most wells, this is true for aluminum. However, Wells 11 and 12 are characterized by feldspar-rich sands. This is true to a lesser degree for Well 4. In fact, for all three of these wells, there is an anti-correlation between clay and non-clay aluminosilicates (feldspars plus micas). The high feldspar content of the sands can be either authigenic as in Well 11 or detrital as in Well 12.

In spite of vast geological differences, Wells 11 and 12 show similar patterns in terms of aluminum vs clay. This suggests that a common algorithm might exist to interpret clay content in these wells, and if so, it might be broadly applicable to feldspar- or mica-rich sands. The relationship determined by least absolute error optimization on the combined Well 11 and Well 12 data sets is:

$$\text{Clay}_2 = -20.8 + 3.1(100 - \text{SiO}_2 - \text{CaCO}_3 - \text{MgCO}_3 - 1.99\text{Fe}) \quad (5)$$

This differs from equation (4) by modifying the slope and introducing an intercept. The results for Wells 11 and 12 are compared to measured clay in Figure 12. Data from Well 4, which also has moderately feldspar-rich sandstones, are included as different symbols; this well was not included in the optimization. Equation (5) for feldspar-rich sandstones gives good results despite the fact that these wells are from very different geological environments.

Estimating Carbonate. The second component in this lithological description is the carbonate fraction. The carbonate fraction will be determined from calcium, but first we need to consider the calcium concentration which we obtain from log data. Pure calcite (CaCO_3) formations have Ca concentrations of 40 wt%, and this concentration is accurately reflected by log data. A complication arises in dolomites ($\text{CaMg}(\text{CO}_3)_2$) because magnesium has not normally been detected by spectroscopy logs. As a result, the log calcium concentration in a pure dolomite is also 40 wt% (see Hertzog et al., 1987 and Roscoe et al., 1995 for detecting Mg from logs). This is equivalent to saying that the Ca detected by logs equals $\text{Ca} + 1.455\text{Mg}$, an expression that equals 40 wt% in either pure calcite or dolomite. Using the core data base, calcite plus dolomite concentrations were optimized as a function of $(\text{Ca} + 1.455\text{Mg})$ to produce equation (6):

$$\text{Calcite} + \text{Dolomite} = -7.5 + 2.69(\text{Ca} + 1.455\text{Mg}). \quad (6)$$

Here, the non-zero offset of -7.5 wt% accounts for the small calcium contribution from plagioclase feldspar in sandstones. The carbonate estimate from equation (6) closely approximates the sum of calcite plus dolomite from all 12 wells (Figure 13) with a correlation coefficient of 0.98. A distinction of calcite from dolomite is possible with the inclusion of magnesium (Hertzog et al., 1987; Roscoe et al., 1995).

The Q-F-M Remainder. The third component of the new lithological description is the sand fraction composed primarily of quartz, feldspars and micas (Q-F-M). This fraction is determined by subtracting the clay and carbonate fractions from 100 wt%.

The lithology fractions defined here are slightly different than those commonly used in log interpretation. The main difference is that a clay fraction rather than a shale fraction is computed. According to Bhuyan and Passey (1994), shales commonly have about 60 wt% clay minerals and 40 wt% Q-F-M. Using this ratio, a rock with 60 wt% clay is 100 wt% shale. The other difference is that the

values determined here are all on porosity-free (or matrix) basis, and they are weight rather than volume fractions.

APPLICATION TO LOG DATA

The goal of this study is to identify an objective, robust, and efficient means of estimating lithology from spectroscopy logs. The two simultaneous developments that have made this possible are the determination of elemental concentrations from induced gamma ray spectroscopy logs and the derivation of the lithology algorithms presented above.

To apply these relationships using the data from Figures 1 and 2 requires that the clay algorithms be modified to account for the known aluminum interference in the iron measurement. Equations 3, 4 and 5 for computing clay or clay plus mica become:

$$\text{Clay}_L = 1.91(100 - \text{SiO}_2 - \text{CaCO}_3 - 1.99\text{FeAl}) \quad (7)$$

$$\text{Clay} + \text{Mica}_L = 2.43(100 - \text{SiO}_2 - \text{CaCO}_3 - 1.99\text{FeAl}) \quad (8)$$

$$\text{Clay}_2_L = -18.5 + 3.34(100 - \text{SiO}_2 - \text{CaCO}_3 - 1.99\text{FeAl}) \quad (9)$$

where the L subscript designates the application to log data. FeAl designates the quantity that would be detected as iron by a spectroscopy device and is equal to $\text{Fe} + 0.14\text{Al}$.

The clay, carbonate and Q-F-M fractions calculated using the Figure 1 openhole spectroscopy data from Well 8 are presented in Figure 14. Also shown are the core clay, carbonate and Q-F-M fractions determined from the FT-IR mineralogy. The agreement between core and log data is quite good, in spite of the fact that Well 8 is probably the worst example of the Al-clay relationship.

The interpretation of the cased hole spectroscopy logs from Well 3 (Figure 2) is presented in Figure 15. The agreement between core and log data is quite spectacular considering that these measurements are made with a 1 1/4-in. diameter tool through casing and cement.

CONCLUSIONS

The quantitative lithology presented here has been optimized on core data from numerous wells from around the world. The lithological fractions of clay, carbonate and quartz-feldspar-mica are ideally suited for the elemental concentration logs of silicon, calcium and iron, which can be acquired by single, induced gamma ray spectroscopy logs. These elemental concentration logs could be available in both open and

cased hole. The strength of this elemental approach to estimating lithology lies in the use of major element chemistry as opposed to trace element chemistry which can be so easily impacted by sediment diagenesis, depositional environment, or the spurious introduction of small amounts of heavy minerals. The elements used are major element contributors to the rock-forming minerals. Their concentrations in a given mineral are relatively stable, and the minerals in which they occur are generally abundant.

The Si-Ca-Fe aluminum emulator gives a demonstrably superior clay interpretation compared to that available from gamma ray. Its strength lies in the near constant slope, small degree of scatter, and near zero intercept. It is also independent of fluid volume, type and density, rendering it free from gas or light hydrocarbon effects, unlike the neutron-density separation.

The calcium log provides an unparalleled carbonate estimation. It provides carbonate quantification in complex lithologies. In heavy barite muds, it easily and accurately locates carbonate cementation at levels of 10 to 20 wt% which were previously undetected by conventional log interpretation.

While the relationships presented here have demonstrated a large degree of universality, each algorithm can be further optimized on a field or regional basis to give improved lithological estimates.

REFERENCES

- Bhuyan, K. and Passey, Q.R., 1994, Clay estimation from GR and Neutron-Density porosity logs, paper DDD, in 35th Annual Logging Symposium Transactions: Society of Professional Well Log Analysts, p. D1-15.
- Ellis, D. V., 1987, *Well Logging for Earth Scientists*: Elsevier, New York, 532 p.
- Grau, J. A. and Schweitzer, J. S., 1989, Elemental concentrations from thermal neutron capture gamma-ray spectra in geological formations: *Nuclear Geophysics*, Vol. 3, No. 1, p. 1-9.
- Grau, J. A., Schweitzer, J. S., Ellis, D. V., and Hertzog, R. C., 1989, A geological model for gamma-ray spectroscopy logging measurements: *Nuclear Geophysics*, Vol. 3, No. 4, p. 351-359.
- Herron, S. L., 1995, Method and apparatus for determining elemental concentrations for γ ray spectroscopy tools, U. S. Patent 5,471,057, November 30.
- Hertzog R. C., Colson, L., Seeman, B., O'Brien, M., Scott, H., McKeon, D., Wraight, P., Grau, J., Ellis, D., Schweitzer, J., and Herron, M., 1987, Geochemical logging with spectrometry tools, SPE-16792. in 62nd Annual Technical Conference and Exhibition Proceedings: Society of Petroleum Engineers.
- Hurst, A. and Milodowski, T., 1994, Characterization of clays in sandstones: Thorium content and spectral log data, paper S, in Sixteenth European Formation Evaluation Symposium: Society of Professional Well Log Analysts.
- Katahara, K. W., 1995, Gamma ray log response in shaly sands: *The Log Analyst*, v. 36, p. 50-55.
- Matteson, A. and Herron, M. M., 1993, Quantitative mineral analysis by Fourier transform infrared spectroscopy, Society of Core Analysts Technical Conference, August 9-11, 1993, SCA 9308.
- Roscoe, B., Grau, J., Cao Minh, C., and Freeman, D., 1995, Non-conventional applications of through-tubing carbon-oxygen logging tools, paper QQ, in 34th Annual Logging Symposium Transactions: Society of Professional Well Log Analysts.
- Schweitzer J. S., Ellis, D. V., Grau, J. A., and Hertzog, R. C., 1988, Elemental concentrations from Gamma-ray spectroscopy logs. *Nuclear Geophysics*, Vol. 2, No. 3, p. 175-181.

E

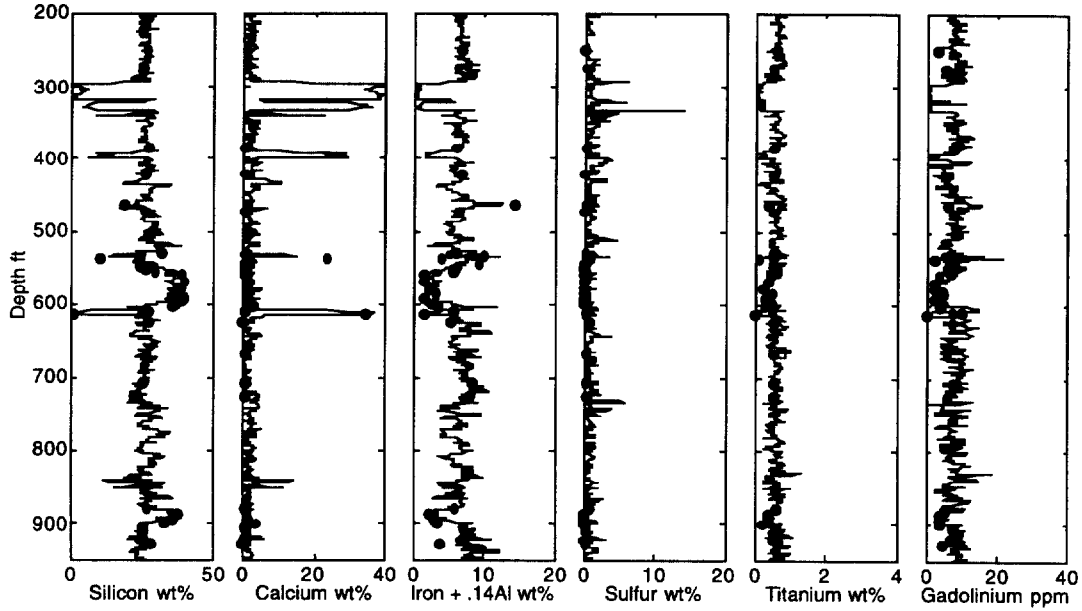


Figure 1. Openhole elemental concentrations from the Elemental Capture Spectroscopy (ECS[®]) sonde.

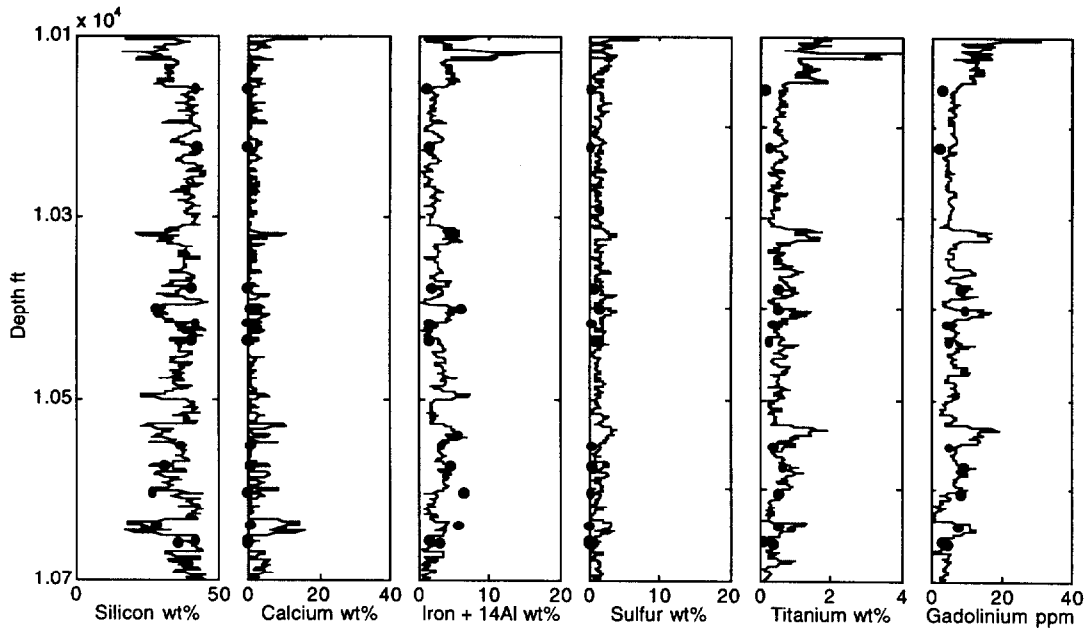


Figure 2. Cased hole elemental concentrations from the (RST[®]) Reservoir Saturation Tool.

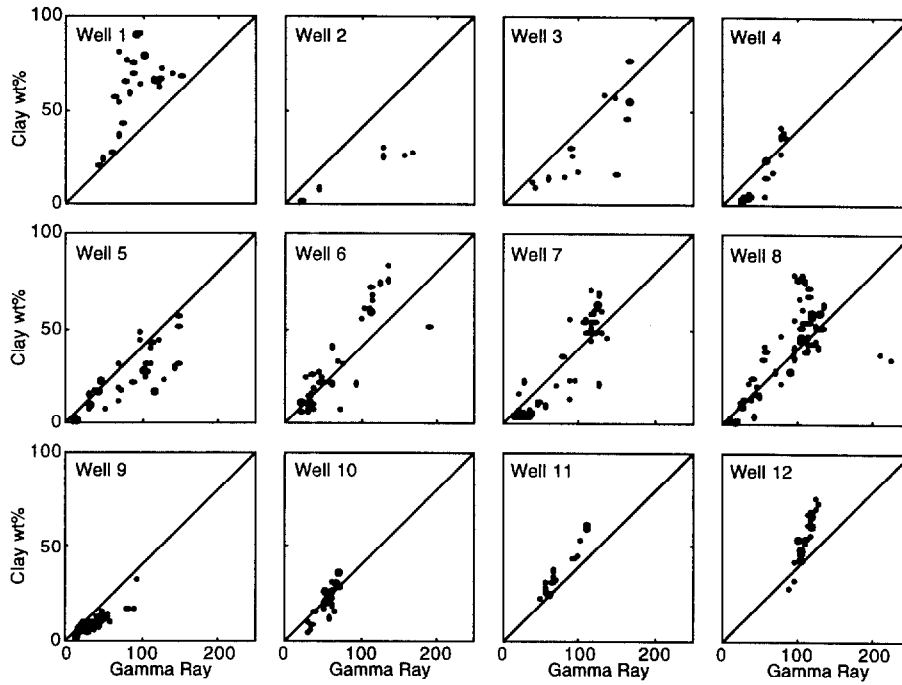


Figure 3. Synthetic gamma ray (computed from Th, U and K concentrations) plotted against total clay (kaolinite, illite, smectite, chlorite and glauconite) measured on the same sample for 12 data sets. Although GR crudely correlates with total clay, the slopes and offsets vary widely from well to well.

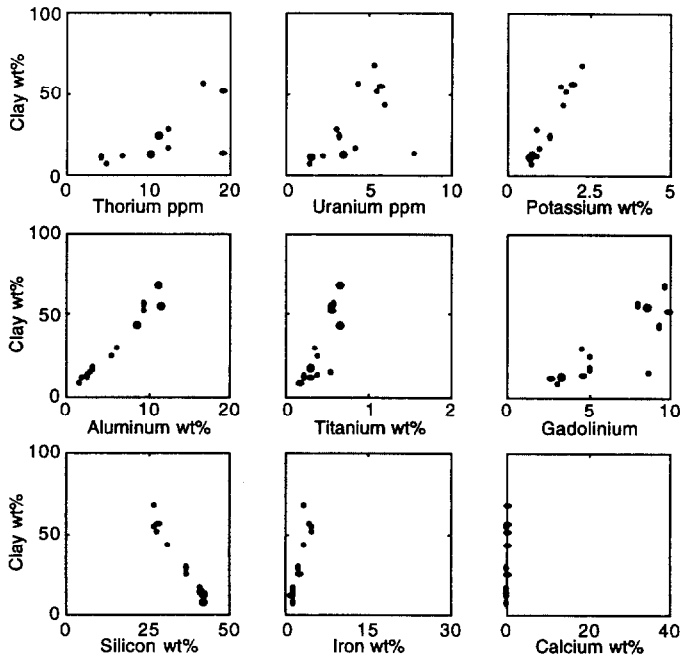


Figure 4. Comparison of individual chemical elements that can be measured by logging against total clay for Well 3. Al shows a strong positive correlation that is mirrored by the negative correlation with Si.

E

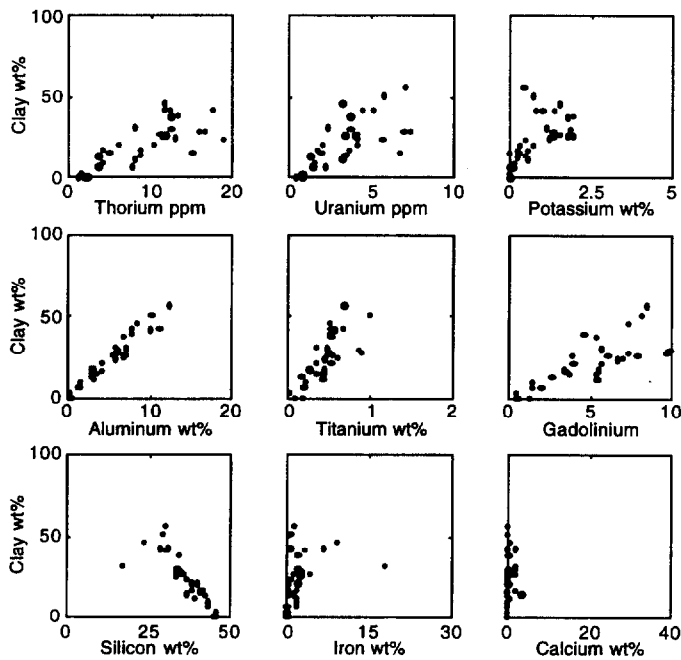


Figure 5. Comparison of individual chemical elements that can be measured by logging against total clay for Well 5. Al again shows a strong positive correlation with clay. The negative correlation with Si is slightly perturbed by high Fe siderite samples.

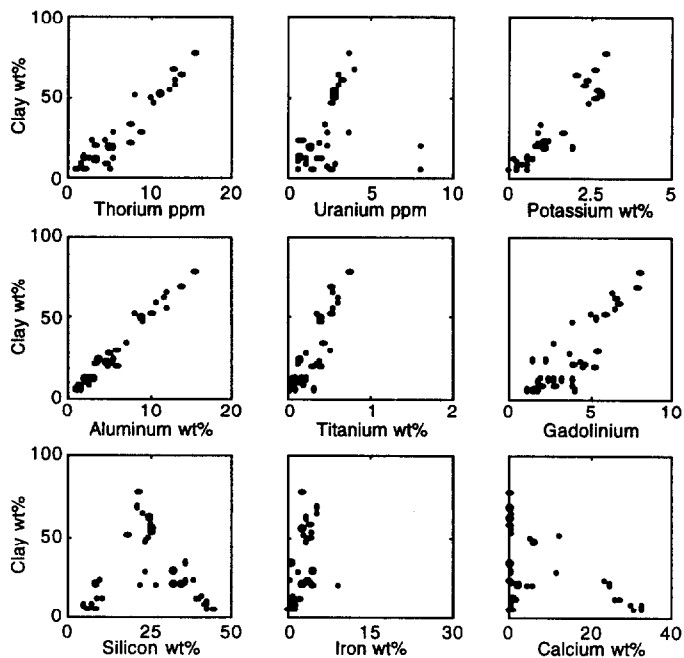


Figure 6. Comparison of individual chemical elements that can be measured by logging against total clay for Well 6. Al shows a strong positive correlation. The anticorrelation with Si is significantly perturbed by carbonates.

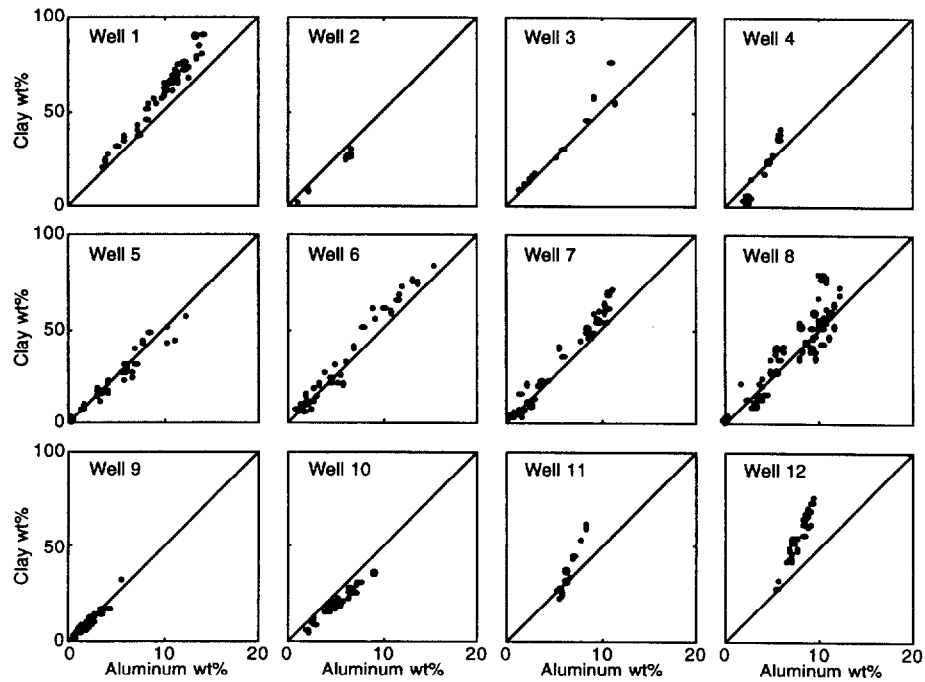


Figure 7. Aluminum versus total clay for all 12 wells. The correlation with total clay is much tighter for aluminum than for GR. In addition, the slopes are about the same and most wells show a near-zero offset.

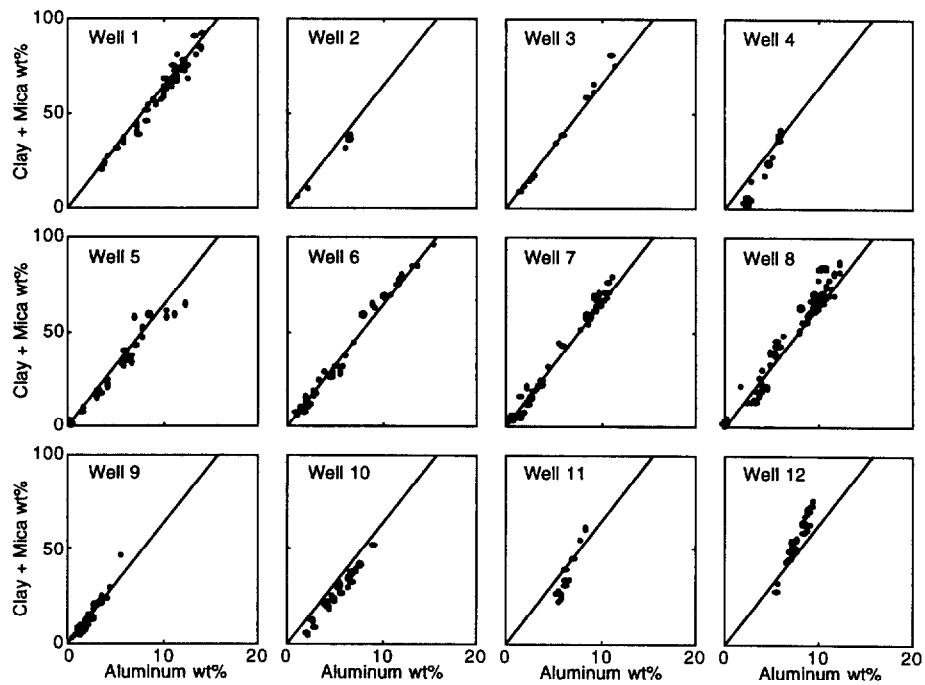


Figure 8. Aluminum versus total clay + mica for all 12 wells shows an even tighter and more universal relationship than aluminum versus clay.

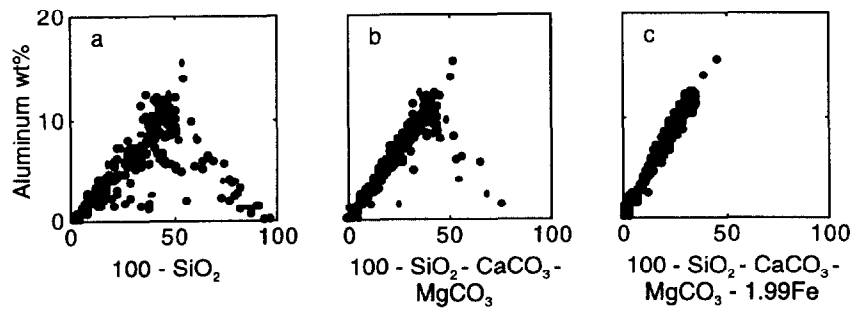


Figure 9. Aluminum is estimated from the other major elements in sedimentary rocks. a) Al vs. $100 - \text{SiO}_2$ shows a clear trend that is disturbed primarily by carbonates. b) Al vs. $100 - \text{SiO}_2 - \text{CaCO}_3 - \text{MgCO}_3$ shows a very tight trend that is disturbed only by siderite and pyrite rich samples. c) When the high-Fe minerals are corrected for, Al can be estimated from Si, Ca and Fe.

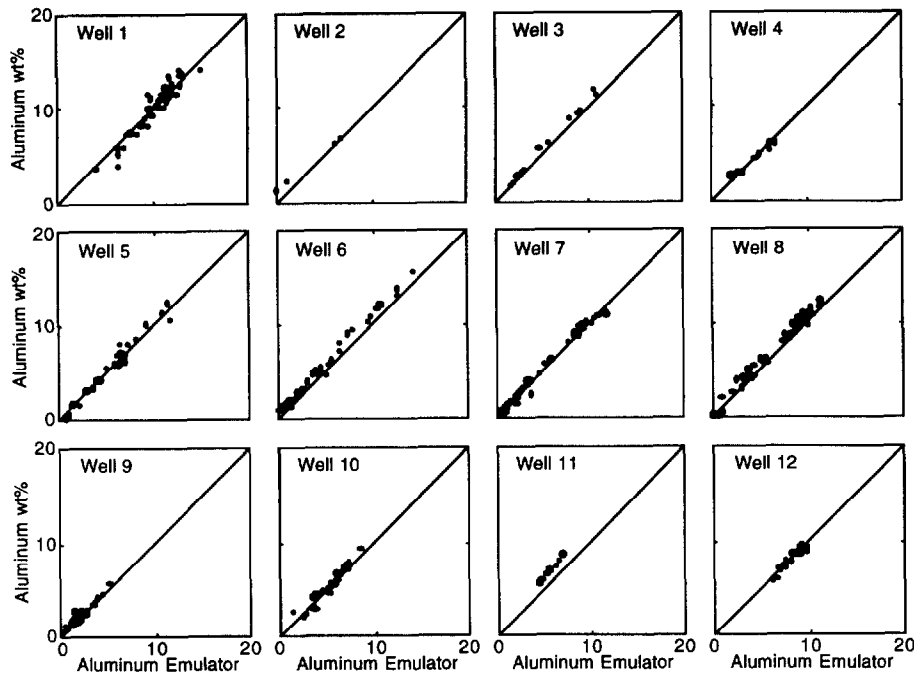


Figure 10. Aluminum estimated from Si, Ca, Mg and Fe closely matches measured aluminum in all 12 wells.

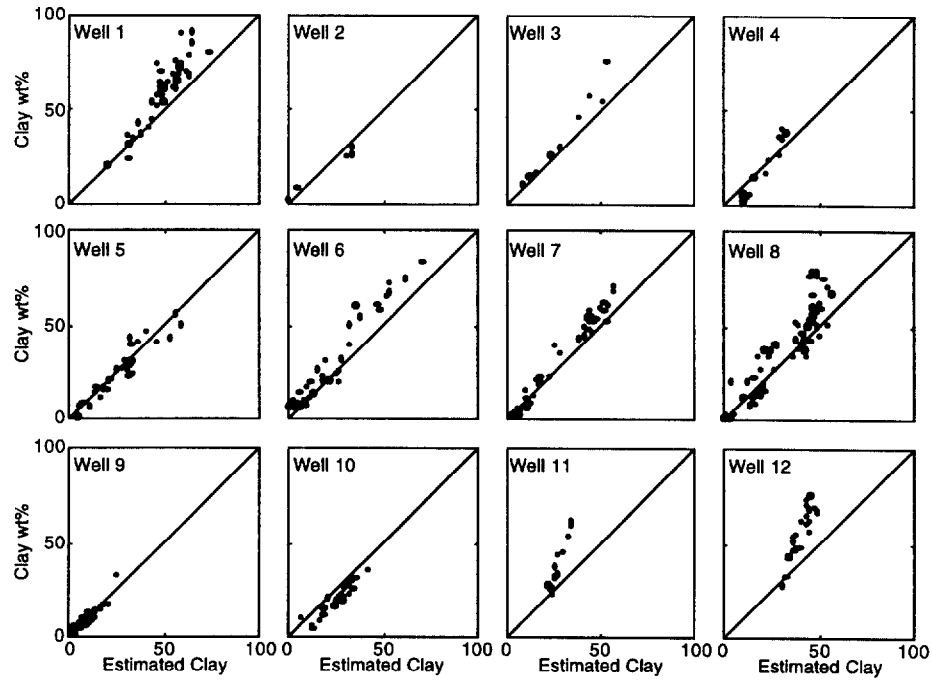


Figure 11. Clay estimated from Si, Ca, Mg and Fe plotted against total clay for all 12 wells is a near duplicate of Figure 7.

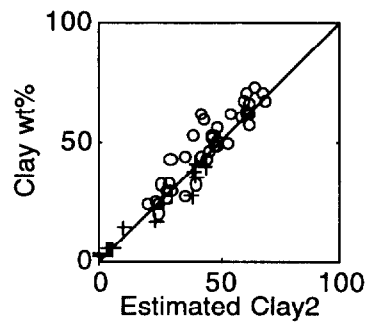


Figure 12. Clay estimated from equation (5) for feldspar-rich sands and shales vs. measured clay for Wells 11 and 12 (o) and Well 4 (+).

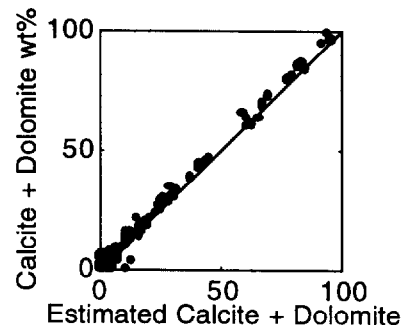


Figure 13. Calcite plus dolomite estimated from equation 6 vs. measured calcite plus dolomite for all twelve wells.

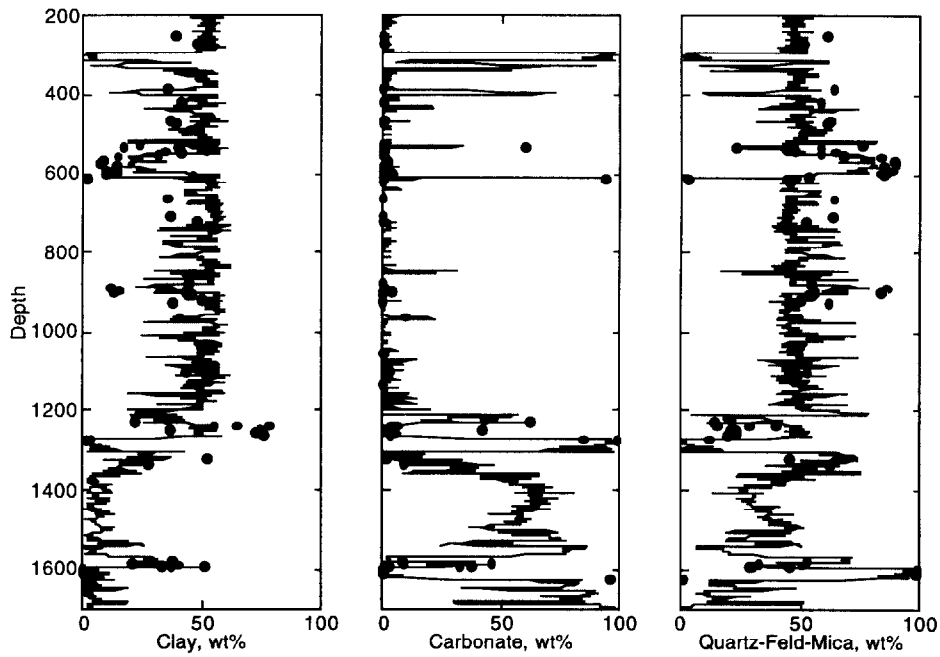


Figure 14. Quantitative lithology logs for Well 8 using the openhole elemental concentration logs shown in Figure 1. FT-IR core measurements are provided for comparison.

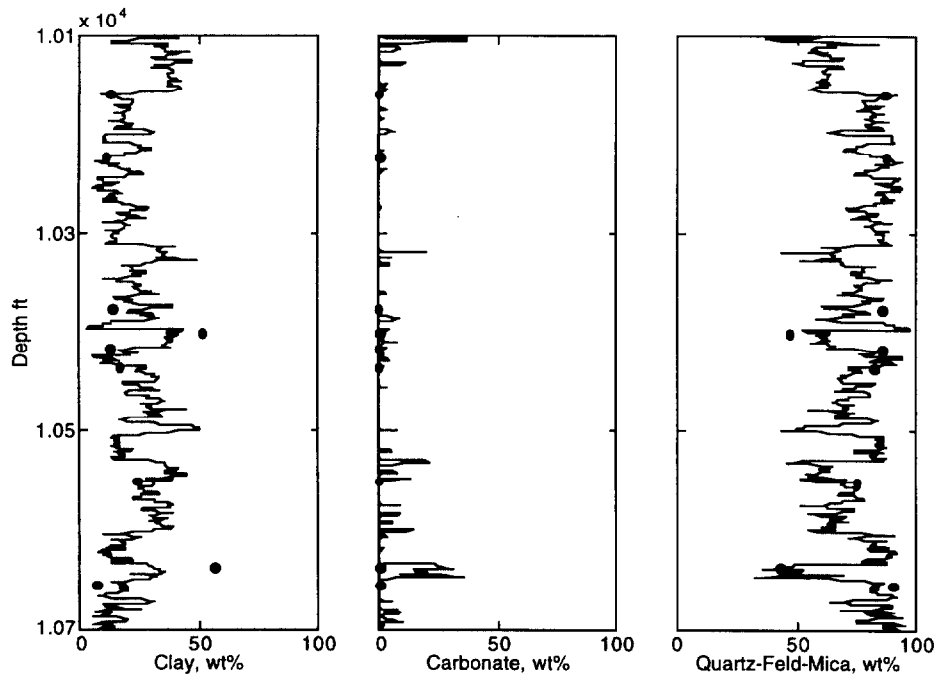


Figure 15. Quantitative lithology logs for Well 3 using the cased hole elemental concentration logs shown in Figure 1. FT-IR core measurements are provided for comparison.